A Blade Motion Simulator for Unsteady Aerodynamic Measurement of Wind Turbine Blades

Mohammad BadrGoltapeh[1]

And

Mohammad Farahani[2]*
Sharif University of Technology, 145888, Tehran, Iran

Abstract

This paper briefly introduces a novel blade motion simulator with a modular and scalable design that has the ability to simulate a combination of both pitching and plunging motions together with the possibility of adding bending or torsional compliances. The device can setup motions while adjusting amplitude, frequency, and time-lag independently. This option makes it possible to simulate both energy-harvesting and propulsive flapping motions. Also, the installation of different torsional and bending compliances with different spring stiffness and orientations can simulate different material properties in order to take aeroelastic effects into account during the motion. Moreover, some results of wind tunnel tests are also presented. These tests demonstrate that the oscillatory motion generated by the simulator largely conforms to the desired motion programmed into the device. Also, the results of measuring the lift coefficient have been compared with Theodorsen's theory, and a good accuracy has been observed. Also, in the following, as a practical example of the performance of the device for a specific case, the hysteresis loop of forces and torque of a blade has been analyzed and investigated.

Keywords: Unsteady Aerodynamics, Wind-tunnel Testing, Wind Turbine, Motion Simulator, Airfoil

[1] Department of Aerospace engineering, Sharif University of Technology, Azadi street, Tehran, +989107787608
[2] Department of Aerospace engineering, Sharif University of Technology, Azadi street, Tehran, +989125123566

Nomenclature

c	=	blade section chord length, m
C_D	=	pressure drag coefficient
C_L	=	lift coefficient
C_M	=	moment coefficient about blade section quarter chord
f	=	oscillation frequency, Hz
h	=	blade model position in perpendicular direction to the motion, m
k_b	=	blade bending stiffness, N/m
k_t	=	blade rotational stiffness, $N.m/rad.$
t	=	time, s
U_∞	=	freestream velocity, m/s
α	=	blade section angle of attack, deg.
φ	=	phase angle, deg.
ω	=	$2\pi f$, oscillation angular frequency, $rad./s$

I.Introduction

The growing increase of energy consumption in the world, threat of environmental pollution, surcease of fossil energy sources together with the necessity of possession of alternative energy sources for industries, increased the application of various renewable energy sources including wind energy. Despite the many advantages of wind power, it must compete with other conventional energy resources on a cost and efficiency basis. One of the most important parts of wind energy generators are blades, that should convert the kinetic energy of the incoming air to mechanical power efficiently. During the recent 30 years, the power and the rotor diameter of the wind turbines have been increased from $10\,kWs$ and $10-15\,m$ to several MW and $\approx 160\,m$, respectively. The blade of every types of wind turbines, ranging from HAWTs to Darrius type VAWTs and flapping foil energy harvesters, experience high amplitude angle of attack alteration. Also, the unsteadiness of the incoming flow, together with the length of the megawatt HAWT blades, leads to the unsteadiness of blade aerodynamics and aeroelastic deformations along the blade. Moreover, flapping foil wind energy harvesters have been gaining attention in recent years and several theoretical and numerical studies have been

performed on them [1 – 9]. The blade of these devices experiences a combination of pitching and plunging motions called flapping [10]. Investigation of the unsteady aerodynamics and aeroelastic behavior of the blade element has a game-changing role in the development and optimization of wind energy generators. Numerous numerical and experimental investigations on different aspects of the wind turbine and heaving foil unsteady aerodynamics have been performed during the recent years. Some distinguished review articles have been published on these efforts [11 – 16].

The unsteady aerodynamics of wind turbine rotors leads to the alteration of aerodynamic forces and structural oscillations [17]. Generally speaking, blade rotation (collective and cyclic blade pitch), geometric twist angle, elastic torsion and bending of blade, flapping motion, induced downwash of nearby blades, blade leading edge perturbation in high angles of attack and alterations of incoming air flow leads to two general flow unsteadiness in the wind turbine aerodynamics, which are time variations of effective angle of attack and velocity field changes [18 – 19]. All the complex unsteady flows around a rotating blade element are modelled with four simplified problems, which are blade section pitching and plunging, variation of incoming flow velocity called lead-lag, and vertical gust flow [19]. The pitching motion models the rotation of the blade and elastic torsions, the plunging motion relates to elastic bending of the blade, lead-lag problem is about the sudden storms and horizontal alternation of incoming flow, and vertical gusts are generated by the induced downwash from the blade tip or downwash of the other blades. Numerous simulations and experiments are performed on these simplified problems of oscillating blade sections to understand different aspects of wind turbine unsteady aerodynamics [20 – 25].

Numerical methods cannot predict all aspects of complex flow-field around an oscillating airfoil, especially when it comes to the measurement of boundary-layer transition, wake, flow control effects, and fluid-solid interactions (aeroelastic features of blade). Therefore, wind-tunnel or field measurement of aerodynamics and aeroelastic features of 3D blade or blade sections have been always of great interest. Several researches are performed, using oscillating

mechanisms to model the pitching and/or plunging motion of airfoils, wings, or blades in the wind tunnel studies. DC servo motor in connection with flywheel and linkages was used to prepare the pitching and plunging motion. The model is attached to these oscillator apparatuses with a spanwise rod, and no external struts or connections were needed inside the test section [26 – 28]. In other researches, pneumatic and hydraulic jacks and are used to convert linear motions to the complicated forced pitching/plunging motion [29 – 30]. A force-measurement unit is also introduced that simulates the flapping motion of a wing in which there is no control on the motion of the model [31]. In some other test rigs, two linear motors are used to produce a pitching/plunging motion. In these instruments, two linear rods connected to the motor transmit the motion to the model, and the difference between the amplitude of the rod displacement produces the compound motions [32 – 36]. Other recent researches use a rack and pinion mechanism to produce a plunging motion [37 – 38]. Numerous test rigs and experimental results are also introduced to measure the dynamic responses of a wing or blade section to the incoming flow in the wind tunnels [39 - 46].

There are some deficiencies in the design of the oscillating apparatuses used in the mentioned research. None of the oscillators used in the above-mentioned literature survey can produce combinations of pitching/plunging motions with separately controllable time-lag and frequencies. It is vital to change the amplitude, frequency, and time difference between the two motions (pitching and plunging) independently in order to study the effects of various parameters on the flow phenomena corresponding to the blade. Even the mechanisms that produce hybrid pitching/plunging motions using linear rods [29 – 33] have no control on the time difference between the motion and the individual frequencies of the motions. Although mechanisms used previously simulate both unsteady aerodynamics and aeroelastic phenomena of wing section or blade, no apparatus can be found that simulates both effects in connection with each other. A useful investigation that can be implemented in the field of fluid-solid interaction of oscillating blades is the measurement of induced plunging motion during a forced pitching motion and vice versa. A HAWT blade oscillates with a known angular velocity, and a low amplitude, high frequency elastic bending or pitching is induced in the blade.

It could be called the future of fluid-solid interactions measurement of oscillating wings or blades. Another flaw of the aforementioned rigs that restrict their use in a variety of applications and different scales is the lack of modularity and scalability of their designs. It can be seen that the existing devices only bear moderate forces, and the designs is not flexible for heavy-duty refinement without any substantial redesigns. Also, using mechanisms such as slider-crank substantially includes mechanical backlash that makes the time difference control of the motions nearly impossible or at least inaccurate.

This paper aims to briefly introduce a novel blade motion simulator with a modular and scalable design that has the ability to simulate both pitching and plunging motions together with the possibility of adding bending or torsional compliances. The device can set up motions while adjusting amplitude, frequency, and time-lag independently. This option makes it possible to simulate both energy-harvesting and propulsive flapping motions. Also, the installation of different torsional and bending compliances with different spring stiffness and orientations can simulate different material properties in order to take aeroelastic effects into account during the motion. This device can be called an all-in-one apparatus for wind tunnel simulation of real blade unsteady aerodynamics and aeroelastic. A general introduction of system parts together with some design considerations are presented in the following parts. Then, wind tunnel test results for three motions of pure pitch, pure plunge, and combined pitch-plunge motions are presented and discussed briefly. The demonstrated experimental results have not been presented previously in any other studies and from aerodynamic point of view are completely novel.

II.Elastic Blade Motion Description

The general motion of an oscillating elastic blade element can be defined as a combination of pitching $\alpha(t)$ and plunging $h(t)$ motions. Restricting to a pitching axis located on the chord line at position x_p from the leading edge, the airfoil motion is expressed as below:

$$\alpha_t(t) = \alpha_0 + \alpha_f(t) + \alpha_e(t) = \alpha_0 + \bar{\alpha}_f \sin(\omega_1 t) + \bar{\alpha}_e \sin(\omega_1' t + \varphi_1) \quad (1)$$

$$h_t(t) = h_f(t) + h_e(t) = \bar{h}_f \sin(\omega_2 t + \varphi) + \bar{h}_e \sin(\omega_2' t + \varphi_2) \qquad (2)$$

where α_0 is the mean angle of attack; $\bar{\alpha}_f$ and $\bar{h}_f$ are, respectively, the forced pitching and plunging amplitude; $\bar{\alpha}_e$ and $\bar{h}_e$ are, respectively, the elastic induced pitching and plunging amplitude; ω_1 and ω_2 are, respectively, the forced pitching and plunging angular frequencies; ω_1' and ω_2' are, respectively, the angular frequency of the elastic induced pitching and plunging motion and φ_1 , φ , and φ_2 are, respectively, the phase difference between elastic pitching motion, forced plunging motion, and elastic plunging motion, with forced pitching motion. Depending on the application under investigation, the above equations can be reduced to a simpler form. For example, in the case of rigid blade of heaving foil energy harvester, the elastic induced motions can be ignored, and ω_1 can be considered equal to ω_2 [1]. Therefore, in general, the motion of an elastic blade element can be characterized with eight independent parameters, as is shown in Table 1. Parameters of induced motion due to aeroelastic effects can be identified by the torsional and bending compliance of the blade which is in relation with material, structural design and manufacturing process. In fact, aeroelastic induced motion parameters can be measured for a blade with specific torsional and bending characteristics in a defined steady or unsteady flow field. It could be concluded that a blade motion simulator should have control on mean angle of attack, pitching and plunging amplitude, frequency and phase difference and bending stiffness (k_b) and rotational stiffness (k_t) of the blade.

III. Blade Motion Simulator

1. Overall Configuration

Figure 1 shows the exploded view of the blade motion simulator. The device consists of two main units of pitching (A) and plunging (B) mechanisms assembled in a columnar arrangement. A plate (B) connects the pitching unit (A) to the lower parts of the machine while converting the rotating motion of the plunge AC motor (i) to linear reciprocating motion. Actually, the rotating motion of the plunge AC motor converts to reciprocating motion with a customized arrangement based on the Scotch Yoke mechanism (also known as slotted link mechanism) [44 – 45]. In this mechanism, the reciprocating part is directly coupled to a sliding yoke with a slot that engages a pin (l) on the

rotating part. The location of the slider versus time, $h(t)$, is a sine wave. The amplitude of the sine wave ($\bar{h}$) is adjusted with a so-called plunge arm adjustment system shown in Fig. 1, and its frequency (ω_2) is controlled by the rotational speed of the plunge servo motor (i). The amplitude of the plunge motion ($\bar{h}$) is adjusted with a linear actuator consists of a DC step motor (k), a linear ball screw (m) and a linear guideway (n) (Fig. 1). A built-in battery and Wi-Fi receiver (j) are also assembled inside the plunge arm adjustment system to supply step motor and control circuit power and receive commands.

2. Blade Motion Simulator Integration with Wind Tunnel

Figure 2 shows the integration arrangement of the blade motion simulator with the wind tunnel test section and blade model. The proposed configuration of the simulator apparatus is appropriate for the vertical installation of the model. The motion simulator locates under test section and blade model connects to the pitching axis with a customized connection device. This device can be designed based on the model connecting screw or spar. This device sits on a standard connecting flange of the pitching axis (Fig. 2a). An electrical panel is also attached to the main frame of the simulator includes motors drivers, PLC, terminals, switches, indicators, and human machine interface. For 2D blade model experiments in which no elastic effects are needed to consider, two towing cable can be connected from the ceiling guideway to the plunging oscillating plate (Fig.1 (B)) to insure the same motion dynamics for the upper and lower points of the model (Fig. 2b, d, and e). Also, for this case, a pitch and plunge motion measurement unit can be installed on the ceiling oscillating plate indicated in Fig.2 d to measure the motion dynamics on the upper part of the model, to ensure the same pitching motion along the model. For 3D models, none of the ceiling motion measurement unit and towing mechanism is needed. In the case of 3D model oscillation (e. g. blade tip), structural vibrations of any points of the model can be measured during the test, using a pair of laser distance sensors or a built-in accelerometer.

3. Bending and Torsional Compliance Add-ons

In order to take the effects of blade material elastic properties into account, two modular add-ons are designed to accommodate the simulator to model bending and torsional compliances. In fact, these add-ons want to alter the parameters regarding the elastic motion in Equations (1) and (2). The application of these parameters is modeling the aeroelastic interactions. Figure 3 shows the integration arrangement of the add-ons with the system and detailed view of each add-on. Bending compliance mechanism as is shown in Fig. 3b consists of a support, a linear guide system, a pair of linear springs of specified stiffness (k_b), a slider, and a linear potentiometer. Mechanism support sits on the plunge oscillating plate (Fig.1 (B)), and pitch mechanism units attach to the slider. The springs can be designed for each structural elastic condition and easily replaced. The torsional compliance unit is shown in Fig. 3c. This mechanism is inspired by the automobile clutch mechanism. It consists of an outer disk and an inner disk connecting with a set of springs and fasteners. The shaft hollow in the center of the system is in connection with the inner disk and connects the torsional compliance mechanism to the pitch mechanism unit (Fig.1 (A)) shaft, and the model attaches to the outer disk. A casing is installed to cover the compliance assembly. The number of springs, their stiffness, and springs placement configuration should be selected to achieve the desired rotational stiffness (k_t).

4. Automation and Control

The mechanism uses a $7.5kW$ AC motor and a $1.8kW$ servo motor, which are responsible for operating plunge and pitch motions, respectively. The AC motor is equipped with a 14-bit angular encoder to provide the ability of close loop motion control. The main control unit of the system is a motion-control PLC. The PLC generates the prescribed sinusoidal motion command for the pitch servo motor, controls the speed of the AC motor, senses the signals of the servo motor and AC motor encoders, controls the time difference between the pitch and plunge axes, and adjusts the initial position of each axis. The settings and commands are applied by the user through a human machine interface (HMI) located on the simulator. The signals of some vibration and proximity sensors monitors in real time and automatic emergency stop or speed reduction commands are generated to ensure safe operation of the system.

IV. Test Setup and Procedure

Experiments were conducted in an open loop, low speed, suction-type wind tunnel with a rectangular test section of $80 \times 100 \times 200 cm^3$. Flow speed in the test section varies continuously from 10 to $100 m/s$, corresponding to Reynolds numbers of 0.6×10^6 to 6×10^6 per meter. Tests were conducted for the current study in the Reynolds number of 0.27×10^6. It should be noted that the tunnel is of an atmospheric type one, and variations of Reynolds number cannot be accomplished through constant Mach number. The nozzle of the tunnel has a $7:1$ contraction ratio and is equipped with a honeycomb and a set of 3 monolith anti-turbulence screens in its settling chamber to reduce the tunnel turbulence level to an acceptable value. The turbulence intensity of the incoming flow in the test section ranges from 0.2% to 1%, depending on the freestream velocity. Measurement inaccuracies of the freestream parameters are listed in Table 2.

A 2D wind turbine blade section model with $25 cm$ chord and $80 cm$ span and a 3D wind turbine blade model with $25 cm$ chord and $60 cm$ span have been used in this investigation. The models have been constructed of fiberglass with a measured accuracy of $\pm 0.1 mm$. The models were installed vertically inside the test section on the wind turbine blade motion simulator as shown in Fig. 2b and e. The accuracy of the angle of attack regulation is 0.0013°. To measure the pressure distribution over the surface of the 2D blade section model, 63 pressure taps were used, congested at the leading edge. For the 3D case, the model is a rectangular blade. 3D model, three rows of pressure taps were located in three different spanwise locations called root-section, mid-section, and tip-section. The airfoil section, in this case, is the critical section of a $660 kW$ wind turbine blade. To measure the pressure distribution over three sections of the model total number of 87 pressure taps were used, congested at the leading edge (29 taps for each section). The surface pressures have been measured using differential pressure transducers with ranges from 0.075 to $1.0 psi$ and maximum uncertainty of 0.15% of full span with a sampling frequency of $1 kHz$.

V. Uncertainty Analysis

In this section, the error of the main motion parameters generated by the simulator is assessed. These parameters are the pitch amplitude ($\bar{\alpha}$), plunge amplitude ($\bar{h}$), pitching reduced frequency (k_1) and plunging reduced frequency (k_2) and the corresponding relative errors are E_1 , E_2 , E_3 and E_4 , respectively. Figure 4 shows these errors for different measured cases. It can be seen that for none of the cases, the relative error is not more than 7% . Also, the error of amplitude and frequency of plunging motion is even lower ($<5\%$). One of the important parameters regarding the errors is dynamic forces. Because of this, several errors may occur for a single pitching or plunging amplitude and frequency.

VI.Wind Tunnel Test Result

1. 2-D wind turbine section

Experiments were conducted in an open loop, low speed, suction-type wind tunnel with a rectangular test section of $80\times100\times200 cm^3$. Tests were conducted for the current study in the Reynolds number of 0.27×10^6 . It should be noted that the tunnel is of an atmospheric type one, and variations of Reynolds number cannot be accomplished through constant Mach number. In these experiments, the turbulence intensity of the incoming flow in the test section ranges from 0.2% to 1% , depending on the free stream velocity. Further details, including wind tunnel specifications, measurement tools, methods, and accuracies can be found in [47-48]. Effective angle of attach corresponding to a combined pitch-plunge motion is calculated as below:

$$\begin{aligned}\alpha_{eff}(t) &= \alpha_0 + \alpha_p(t) + \alpha_{eq}(t) = \alpha_0 + \bar{\alpha}\sin(\omega_1 t) + ton^{-1}\left(\frac{-\dot{h}}{U_\infty}\right) \\ &= \alpha_0 + \bar{\alpha}\sin(\omega_1 t) + ton^{-1}\left(\frac{-\omega_2 \bar{h}\cos(\omega_2(t+\varphi))}{U_\infty}\right)\end{aligned} \tag{3}$$

Figure 5 compares the measured equivalent angles of attack with analytical formulas. The results show a good fit between the movement produced by the simulator and the theoretical movement set in the device. Also, this figure compares the experimental results of lift coefficient with the predicted values obtained by Theodorsen theory for a combined pitch-plunge motion with pitch amplitude of 2 degrees, pitch frequency of $2.55 Hz$, plunging amplitude of

$0.44m$ and plunging frequency of $1.02Hz$ at zero-degree angle of attack and freestream velocity of $20m/s$. Theodorsen derived a related model to study the aeroelastic problem of flutter instability [49]. Theodorsen's model is an unsteady extension of the quasi-steady thin airfoil theory to include added-mass forces and the effect of wake vorticity. Further details on this theory can be found in [47 – 48]. Also, a brief overview of the Theory and its extensions can be found in [50].

Fig. 6 shows the measured hysteresis of aerodynamic coefficients for three motions of pure pitch, pure plunge and combined pitch-plunge with mean angle of attack of 10 degrees in freestream velocity of $20m/s$. The aerodynamic coefficients are calculated by the integration of the measured surface pressure as proposed by J. D. Anderson [48]. As it is shown in Figure 6, the values for pitch frequency, pitch amplitude, plunge frequency, and plunge amplitude are $2.55Hz$, 5 degrees, $1.02Hz$, and $62mm$, respectively. The equivalent pitch amplitude of the plunge motion is 1.138 degrees. The frequencies, amplitudes, and phase lag of oscillations remained the same in the combined pitch-plunge motion. The effective angle of attack formulation, together with its variations versus time for each motion, is shown on the top of each motion column. For combined pitch-plunge motion red line is the variation of pitch angle ($A(t)$), the blue line is the variation of plunge effective angle of attack ($B(t,\varphi)$), and the black line is the summation of both. The aforementioned motion is not necessarily related to a common motion of a blade but is selected to show different aspects of the blade motion simulator capabilities. In this test case, all the parameters of the motion are independently configured, which is the main technical capability achievable with the current motion simulator that has been inaccessible before. Also, this figure shows that the super-position of pitching and plunging motions can affect the configuration of force hysteresis. For pure pitching lift, hysteresis is narrow in lower angles of attack but becomes thicker as angle of attack increases. Superposition of the pitching and plunging motion makes the width of the loop constant all over the cycle. It greatly depends on the amplitudes of pitching and plunging motions and the time-lag between them. For drag force, the effect of superposition leads to the change in the orientation of the loop in lower

angles of attack. Generally, it could be said that the aerodynamic response of a pitching-plunging motion greatly affected by the amplitudes, frequencies and the time-lag between the motions.

2. 3-D wind turbine blade model

The popular method for the calculation of lift coefficient variation of a 2D airfoil undergoing simple harmonic motion has been based on the Theodorsen model. To verify dynamic experimental results, this method has been used for comparison. Theodorsen introduced a mathematical model in which both the airfoil and its shed wake are represented by a vortex sheet, with the wake extending as a planar surface from the trailing edge downstream to infinity. The assumption of a planar wake is justified if the angle of attack disturbances remains relatively small. Theodorsen solved the unsteady airfoil problem for simple harmonic motion in a form that represents a transfer function between the forcing and the aerodynamic response. It could be proved that for a combination of two general simple harmonic motions of pitch (around $c/4$) and plunge with a reduced frequencies of k, Theodorsen's model gives the lift coefficient as:

$$C_L = 2\pi C(k)\left[\alpha + \frac{c\dot{\alpha}}{2U} - \frac{\dot{h}}{U}\right] + \frac{\pi c}{2}\left[\frac{\dot{\alpha}}{U} - \frac{\ddot{h}}{U^2} + \frac{c\ddot{\alpha}}{4U^2}\right] \quad (4)$$

Where α and h are instantaneous pitch angle and plunge position, respectively. Theodorsen's transfer function $C(k)$ is expressed in terms of two modified Bessel functions of the second kind and is given by

$$C(k) = Me^{i\psi_n} = \frac{K_1(ik)}{K_0(ik) + K_1(ik)} \quad (5)$$

Figure 7 and Figure 8 compares time evolution and hysteresis loops of measured and calculated lift coefficients for a plunging motion with $\bar{h}/c = 0.1$, $k = 0.07$ and zero mean angle of attack. Theodorsen lift

model calculates the unsteady part of the lift response, so the zero-mean value of the measured lift coefficient is used for comparison, which is denoted as C_L^* in the rest of the paper. This parameter shows the unsteady features of the lift coefficient regardless of mean value. Also, the measured lift coefficient is interpolated with a simple harmonic function using a zero-mean filter (ZMF). The mean filter helps us to qualitatively compare the measured sectional lift coefficient value with the measured 2D and Theodorsen values in terms of slope and amplitude. These figures show that the experimental lift values are appropriately close to the Theodorsen theory results even in root and middle sections of the 3D model. However, for the tip-section, Theodorsen theory which has a root in thin airfoil theory fails to accurately predict the lift response amplitude. This outcome is expectable regarding wing tip effect. The tip section is greatly affected by tip vortices. But, still Theodorsen theory accurately predicts the phase of the lift response.

Experimental results are not exactly simple harmonic and some deviations from the sinusoidal function is seen. This leads to a lift hysteresis that deviates from the common elliptical shape. The slope of the lift hysteresis is also much lower for the tip section, which leads to decreased lift amplitude. It means that the flow field near the tip of the model is affected by body motion less than the middle and root sections.

VII.Conclusions

The design of a blade oscillating motion simulator is described in detail. In addition, the various parts of this device and how they are related to each other and how they are designed are discussed, and some results of wind tunnel tests are also presented. These tests demonstrate that the oscillatory motion generated by the simulator largely conforms to

the desired motion programmed into the device. Also, the results of measuring the lift coefficient have been compared with Theodorsen's theory, and a good accuracy has been observed. Also, in the following, as a practical example of the performance of the device for a specific case, the hysteresis loop of forces and torque of a blade has been analyzed and investigated. A suggestion for future research is to add closed-loop control capability to adjust motion parameters with changes in dynamic forces. This could significantly errors of the generated motion.

References

[1] Kinsey, T., and Dumas, G., "Parametric study of an oscillating airfoil in a power-extraction regime", *AIAA Journal*, Vol. 46, No. 6, 2008, pp. 1318 - 1330. [DOI: 10.2514/1.26253]

[2] Deng, J., et al., "Inertial effects of the semi-passive flapping foil on its energy extraction efficiency", *Physics of Fluids*, Vol. 27, No. 5, 2015, pp. 053103. [DOI: 10.1063/1.4921384]

[3] Siala, F., and Liburdy, J. A., "Energy harvesting of a heaving and forward pitching wing with a passively actuated trailing edge", *Journal of Fluids and Structures*, Vol. 57, 2015, pp. 1 – 14. [DOI: 10.1016/j.jfluidstructs.2015.05.007]

[4] Wei, Z. A., and Zheng, Z. C., "Energy-harvesting mechanism of a heaving airfoil in a vortical wake", *AIAA Journal*, Vol. 55, No. 12, 2017, pp. 1 – 13. [DOI: 10.2514/ 1.J055628]

[5] Su, Y., et al., "Confinement effects on energy harvesting by a heaving and pitching hydrofoil", *Journal of Fluids and Structures*, Vol. 84, 2019, pp. 233 – 242. [DOI: 10.1016/j.jfluidstructs.2018.11.006]

[6] Zhao, F., et al., & Tang, H, "Interaction of two fully passive flapping foils arranged in tandem and its influence on flow energy harvesting", *Energy*, Vol. 268, 2023, p. 126714. [DOI: 10.1016/j.energy.2023.126714]

[7] Zheng, M., Hou, G., & Huang, Z, "Energy-harvesting behavior and configuration effect of two semi-active flapping foils", *Physics of Fluids*, Vol. 36, No. 10, 2024. [DOI: 10.1063/5.0225213]

[8] Liu, Z., et al., "Partial confinement effects on the performance of a flapping foil power generator", *Physics of Fluids*, Vol. 35, No. 2, 2023. [DOI: 10.1063/5.0134701]

[9] Li, K., Zhou, D., & Sun, X., "Performance characteristics of flapping foil flow energy harvester that mimics movement of swimming fish", *Ocean Engineering*, Vol. 280, 2023, p. 114850. [DOI: 10.1016/j.oceaneng.2023.114850]

[10] Thiria, B., "On flapping flight mechanisms and their applications to wind and marine energy harvesting", *Current Opinion in Insect Science*, Vol. 30, 2018, pp. 39 – 45. [DOI: 10.1016/j.cois.2018.09.001]

[11] Wang, T., "A brief review on wind turbine aerodynamics", *Theoretical and Applied Mechanics Letters*, Vol. 2, No. 6, 2012, pp. 062001. [DOI: 10.1063/2.1206201]

[12] Snel, H., "Review of aerodynamics for wind turbines", *Wind Energy*, Vol. 6, No. 3, 2003, pp. 203-211. [DOI: 10.1002/we.97]

[13] Kumar, R., Raahemifar, K., and Fung, A. S., "A critical review of vertical axis wind turbines for urban applications", *Renewable and Sustainable Energy Reviews*, Vol. 89, 2018, pp. 281-291. [DOI: 10.1016/j.rser.2018.03.033]

[14] Hansen, M. O. L., and Madsen, H. A., "Review paper on wind turbine aerodynamics", *Journal of Fluids Engineering*, Vol. 133, No. 11, 2011, pp. 114001. [DOI: 10.1115/1.4005031]

[15] Xiao, Q., and Zhu, Q., "A review on flow energy harvesters based on flapping foils", *Journal of Fluids and Structures*, Vol. 46, 2014, pp. 174 – 191. [DOI: 10.1016/j.jfluidstructs.2014.01.002]

[16] Gardner, A. D., et al., "Review of rotating wing dynamic stall: experiments and flow control", *Progress in Aerospace Sciences*, Vol. 137, 2023, p.100887. [DOI: 10.1016/j.paerosci.2023.100887]

[17] Hansen, M. O. L., et al., "State of the art in wind turbine aerodynamics and aeroelasticity", *Progress in Aerospace Sciences*, Vol. 42, No. 4, 2006, pp. 285-330. [DOI: 10.1016/j.paerosci.2006.10.002]

[18] Leishman, J., G., *Principles of Helicopter Aerodynamics*, 2nd Ed., Cambridge University Press, Cambridge, UK, 2000, pp. 302-306. [ISBN: 0-521-85860-7]

[19] Akhlaghi, H., Soltani, M. R., & Maghrebi, M. J., "Investigation of time-frequency analysis and transitional boundary layer over a pitching airfoil", *Scientia Iranica*, Vol. 28, No. 2, 2021, pp. 860-876. [DOI: 10.24200/sci.2020.53393.3218]

[20] Leishman, J., G., "Challenges in modelling the unsteady aerodynamics of wind turbines", *Wind Energy*, Vol. 5, No. 2-3, 2002, pp. 85-132. [DOI: 10.1002/we.62]

[21] Tian, W., et al., "An experimental study of the effects of pitch-pivot-point location on the propulsion performance of a pitching airfoil", *Journal of Fluids and Structures*, Vol. 60, 2016, pp. 130-142. [DOI: 10.1016/j.jfluidstructs.2015.10.014]

[22] Soltani, M. R., and Marzabadi, F. R., "Experimental investigation of transition on a plunging airfoil", *Scientia Iranica, Transaction B: Mechanical Engineering*, Vol. 17, No. 6, 2010, pp. 468-479. [DOI: not available]

[23] Mackowski, A. W., and Williamson, C. H. K., "Direct measurement of thrust and efficiency of an airfoil undergoing pure pitching", *Journal of Fluid Mechanics*, Vol. 765, 2015, pp. 524-543. [DOI: 10.1017/jfm.2014.748]

[24] Birch, D., and Lee, T., "Investigation of the near-field tip vortex behind an oscillating wing", *Journal of Fluid Mechanics*, Vol. 544, 2005, pp. 201-241. [DOI: 10.1017/S0022112005006804]

[25] Baik, Y. S., et al., "Unsteady force generation and vortex dynamics of pitching and plunging aerofoils", *Journal of Fluid Mechanics*, Vol. 709, 2012, pp. 37-68. [DOI: 10.1017/jfm.2012.318]

[26] Angulo, I. A., and Ansell, P. J., "Influence of aspect ratio on dynamic stall of a finite wing", *AIAA Journal*, 2019, pp. 1-12. [DOI: 10.2514/1.J057792]

[27] Soltani, M. R., Seddighi, M., and Marzabadi, F. R., "Comparison of pitching and plunging effects on the surface pressure variation of a wind turbine blade section", *Wind Energy*, Vol. 12, No. 3, 2009, pp. 213-239. [DOI: 10.1002/we.286]

[28] Tabrizian, A., M. Masdari, and M. Tahani. "Surface pressure study of an airfoil undergoing combined pitch and low-amplitude plunge motions", *Journal of Applied Fluid Mechanics*, Vol. 12, Mo. 6, 2019, pp. 1957-1966. [DOI: 10.29252/jafm.12.06.29824]

[29] Francis, M. S., Keesee, J.E. and Retelle Jr, J. P., "A Two-degree-of-freedom oscillator for unsteady aerodynamics applications", *FRANK J SEILER RESEARCH LAB UNITED STATES AIR FORCE ACADEMY COLORADO*, No. FJSRL-TR-81-0007, 1981. [DOI: not available]

[30] Lee, T., and Su, Y. Y., "Surface pressures developed on an airfoil undergoing heaving and pitching motion", *Journal of Fluids Engineering*, Vol. 137, No. 5, 2015, p. 051105. [DOI: 10.1115/1.4029443]

[31] Green, R. B., and Galbraith, R. A. M., "Dynamic recovery to fully attached aerofoil flow from deep stall", *AIAA journal*, Vol. 38, No. 8, 1995, pp. 1433-1440. [DOI: 10.2514/3.12565]

[32] Platzer, M. F., et al., "Flapping wing aerodynamics: progress and challenges", *AIAA journal*, Vol. 46, No. 9, 2008, pp. 2136-2149. [DOI: 10.2514/1.29263]

[33] Yuan, W., et. al., "Numerical and experimental simulations of flapping wings", *International Journal of Micro Air Vehicles*, Vol. 2, No. 3, 2010, pp. 181-209. [DOI: 10.1260/1756-8293.2.3.181]

[34] Rival, D., and Tropea, C., "Characteristics of pitching and plunging airfoils under dynamic-stall conditions", *Journal of Aircraft*, Vol. 47, No. 1, 2010, pp. 80-86. [DOI: 10.2514/1.42528]

[35] Rival, D., Manejev, R., and Tropea, C., "Measurement of parallel blade–vortex interaction at low Reynolds numbers", *Experiments in Fluids*, Vol. 49, No. 1, 2010, pp. 89-99. [DOI: 10.1007/s00348-009-0796-1]

[36] Ol, M. V., et al., "Shallow and deep dynamic stall for flapping low Reynolds number airfoils", *Experiments in Fluids*, Vol. 46, No. 5, 2009, pp. 883-901. [DOI: 10.1007/s00348-009-0660-3]

[37] Ghamkhar, K., Ebrahimi, A., and Shariloo, K., "Wavelet analysis of the flow field around an oscillating airfoil undergoing pure pitching motion at low Reynolds number", *Physics of Fluids*, Vol. 35, No. 6, 2023. [DOI: 10.1063/5.0154125]

[38] Ghamkhar, K., and Ebrahimi, A., "Pressure wavelet analysis of pitching oscillating airfoils in tandem configuration at low Reynolds number", *Physics of Fluids*, Vol. 36, No. 9, 2024. [DOI: 10.1063/5.0228652]

[39] McGowan, G. Z., et al., "Investigations of lift-based pitch-plunge equivalence for airfoils at low Reynolds numbers", *AIAA journal*, Vol. 49, No. 7, 2011, pp. 1511-1524. [DOI: 10.2514/1.J050924]
[40] Onoue, K., et al. "Large amplitude flow-induced oscillations and energy harvesting using a cyber-physical pitching plate", *Journal of Fluids and Structures*, Vol. 55, 2015, pp. 262-275. [DOI: 10.1016/j.jfluidstructs.2015.03.004]
[41] Strganac, T. W., et al., "Identification and control of limit cycle oscillations in aeroelastic systems", *Journal of Guidance, Control, and Dynamics*, Vol. 23, No. 6, 2000, pp. 1127-1133. [DOI: 10.2514/2.4664]
[42] Abdul Razak, N., Andrianne, T., and Dimitriadis, G., "Flutter and stall flutter of a rectangular wing in a wind tunnel", *AIAA Journal*, Vol. 49, No. 10, 2011, pp. 2258-2271. [DOI: 10.2514/1.J051041]
[43] Abdelkefi, A., et al., "An analytical and experimental investigation into limit-cycle oscillations of an aeroelastic system", *Nonlinear Dynamics*, Vol. 71, No. 1-2, 2013, pp. 159-173. [DOI: 10.1007/s11071-012-0648-z]
[44] O' Donnell, K., et al. "Design of a wind tunnel apparatus to assist flow and aeroelastic control via zero net mass flow actuators", *48th AIAA/ASME/ASCE/AHS/ASC Structures, Structural Dynamics, and Materials Conference*, 2007. [DOI: 10.2514/6.2007-1771]
[45] De Marqui Junior, C., et al. "Design of an experimental flutter mount system", *Journal of the Brazilian Society of Mechanical Sciences and Engineering*, Vol. 29, No. 3, 2007, pp. 246-252. [DOI: 10.1590/S1678-58782007000300003]
[46] Dos Santos, C. R., Marques, F. D., and Hajj, M. R., "The effects of structural and aerodynamic nonlinearities on the energy harvesting from airfoil stall-induced oscillations", *Journal of Vibration and Control*, Vol. 25, No. 14, 2019. [DOI: 10.1177/1077546319844383]
[47] Daliri, A., Maghrebi, M. J., and Soltani, M. R., "Experimental assessment of Theodorsen's function for uncoupled pitch–plunge motion", *Physics of Fluids*, Vol. 35, No. 3, 2023. [DOI: 10.1063/5.0139918]
[48] Anderson, J. D., *Fundamentals of Aerodynamics*, 6th Ed., McGraw Hill, 2016, p. 26. [ISBN: 978-1259129919]
[49] Martin, G., H., *Kinematics and Dynamics of Machines*, 2nd Ed., Waveland Press, Inc., 2002, p. 29. [ISBN: 978-1478614005]
[50] Feng, L. H., and Wang, T., "Combined Theodorsen and Sears theory: experimental validation and modification", *Journal of Fluid Mechanics*, Vol. 986, 2024. [DOI: 10.1017/jfm.2024.139]

List of Captions:

Tables:

Figures:

Tables:

Table 1 Independent parameters to characterize an elastic blade element motion

Motions	**Forced Pitching**			**Forced Plunging**			**Induced Pitching**			**Induced Plunging**		
	α_0	$\bar{\alpha}_f$	ω_1	$\bar{h}_f$	ω_2	φ	$\bar{\alpha}_e$	ω_1'	φ_1	$\bar{h}_e$	ω_2'	φ_2
Independent Parameters	α_0	$\bar{\alpha}_f$	ω_1	$\bar{h}_f$	ω_2	φ		k_t			k_b	

Table 2 Freestream flow measurement Inaccuracies (%)

$\Delta T/T$	$\Delta P/P$	$\Delta\rho/\rho$	$\Delta U_\infty/U_\infty$	$\Delta \mathrm{Re}/\mathrm{Re}$
0.033	1.421	0.035	2.009	2.010

Figures:

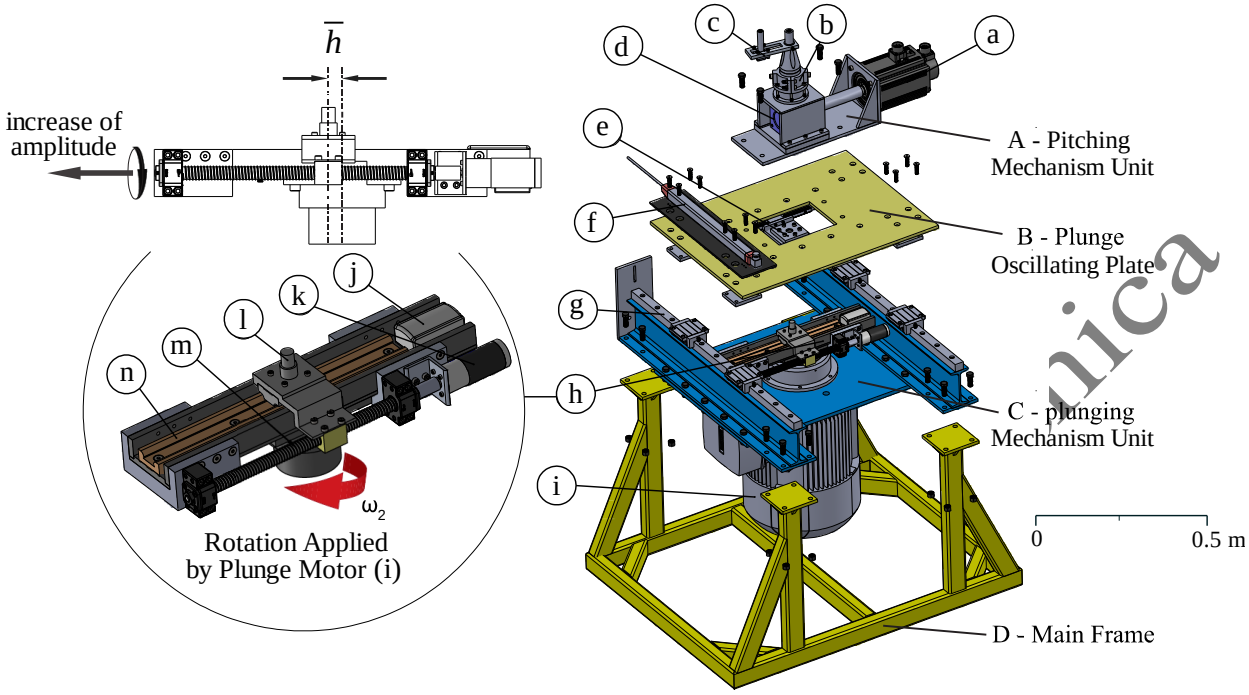

Figure 1 Exploded view of the blade motion simulator, a) pitch servo motor, b) pitch axis brake, c) model holder, d) right angle 1:1 gearbox, e) plunge motion transmission carriage, f) linear potentiometer g) plunge linear guide, h) plunge amplitude adjustment system (PAA), i) plunge motor, j) WiFi receiver k) PAA motor, l) PPA connecting rod, m) linear ball screw, n) PPA linear guide

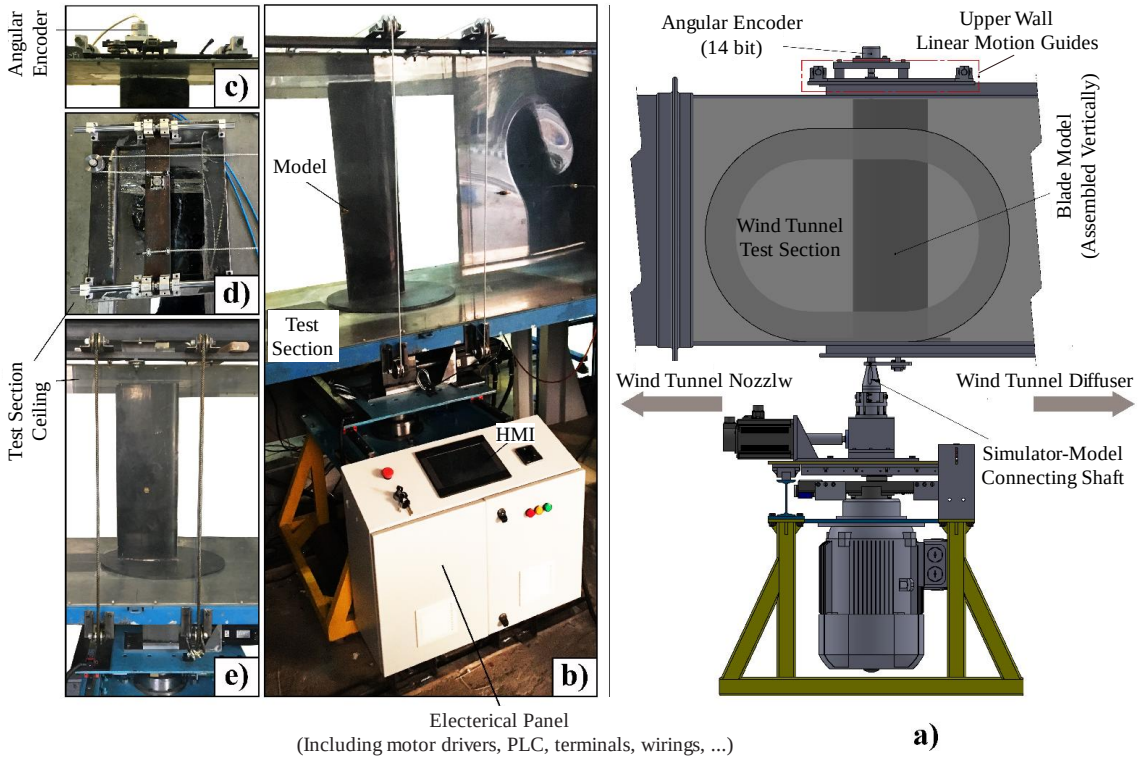

Figure 2 a) Schematic of integration arrangement of blade motion simulator and wind tunnel test section, b) Installation of a 2D blade model on motion simulator integrated with a $1.0m \times 0.8m$ m wind tunnel test section, c) Motion dynamic measurement unit installed on the test section ceiling, d) Ceiling guide way on the test section ceiling necessary for 2D models, e) Tow cable installation arrangement for 2D models

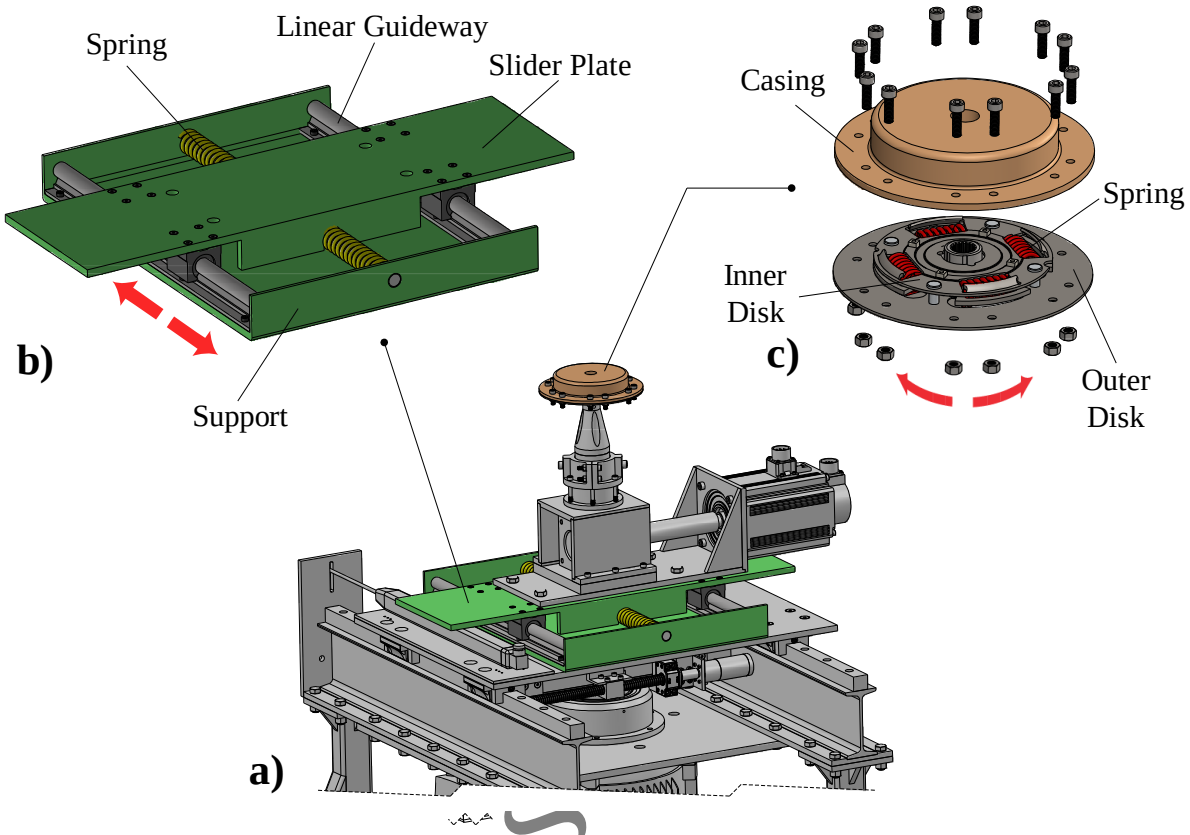

Figure 3 a) Inclusion arrangement of bending and torsional compliances in the basic simulator configuration, b) Bending compliance mechanism, c) Torsional compliance mechanism detail view

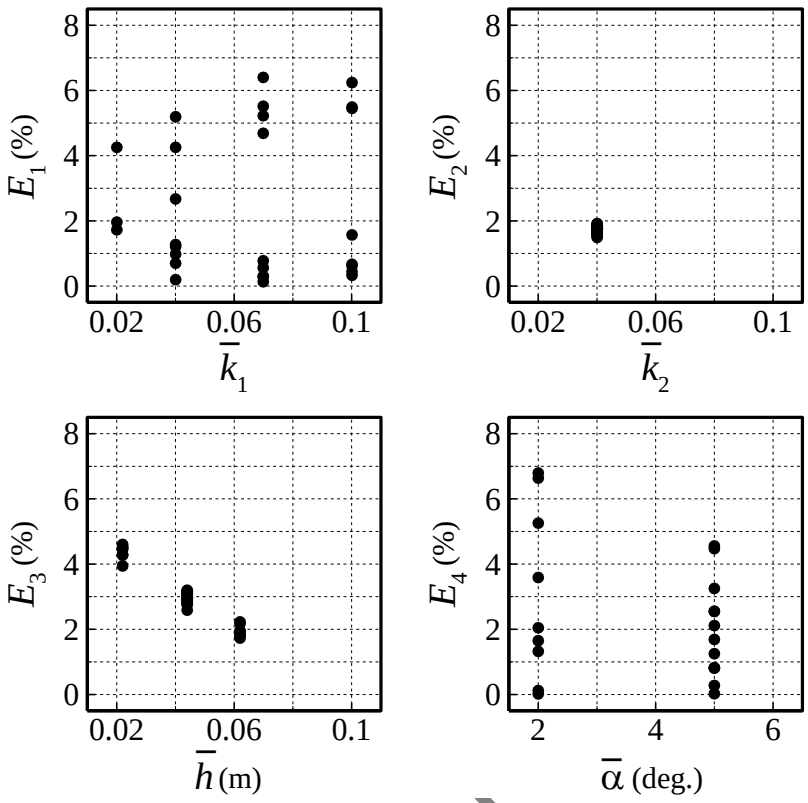

Figure 4 Inaccuracy of motion parameters

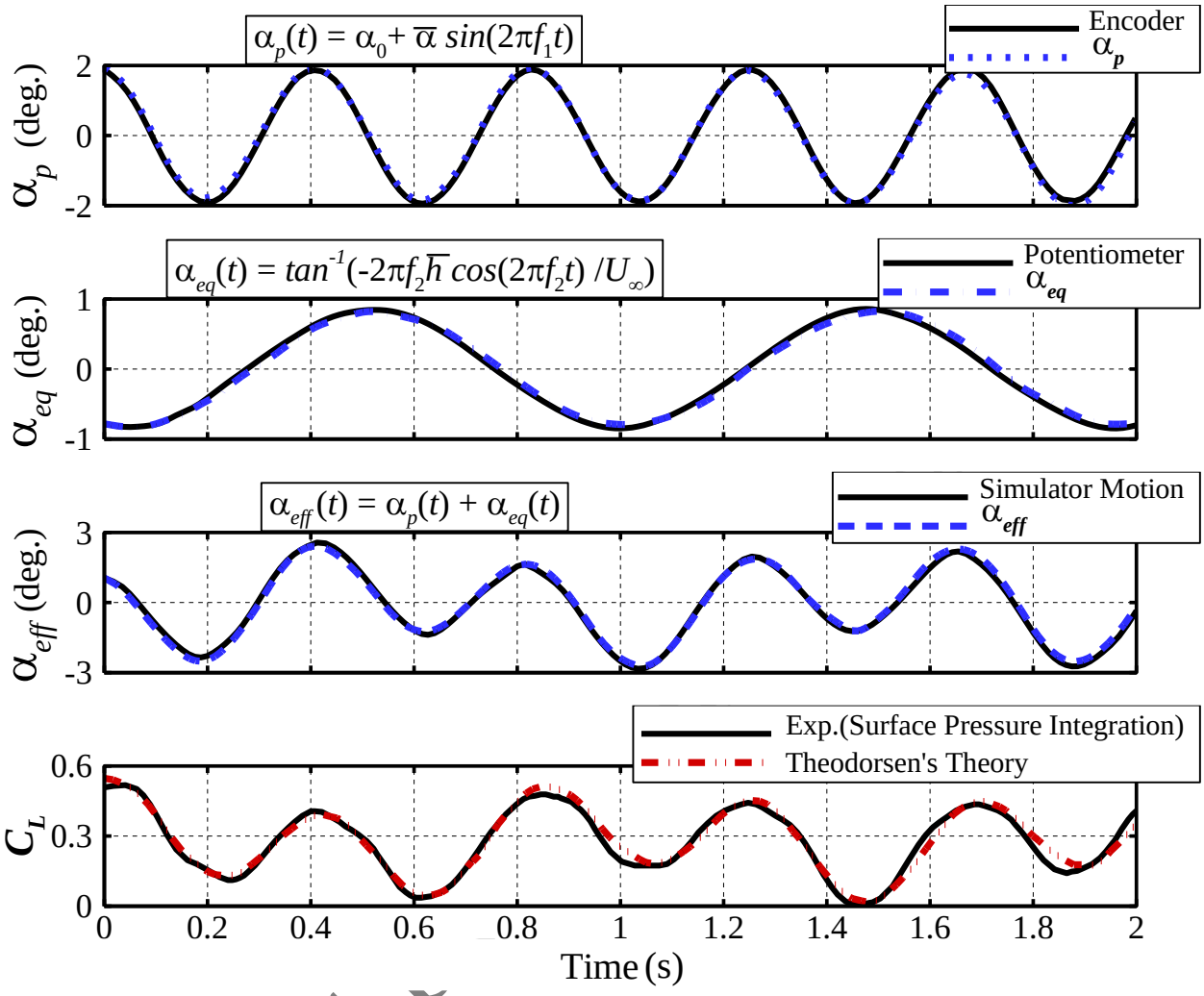

Figure 5 Comparison of measured time history of angle of attacks and lift coefficients with analytical formulations and Theodorsen theory

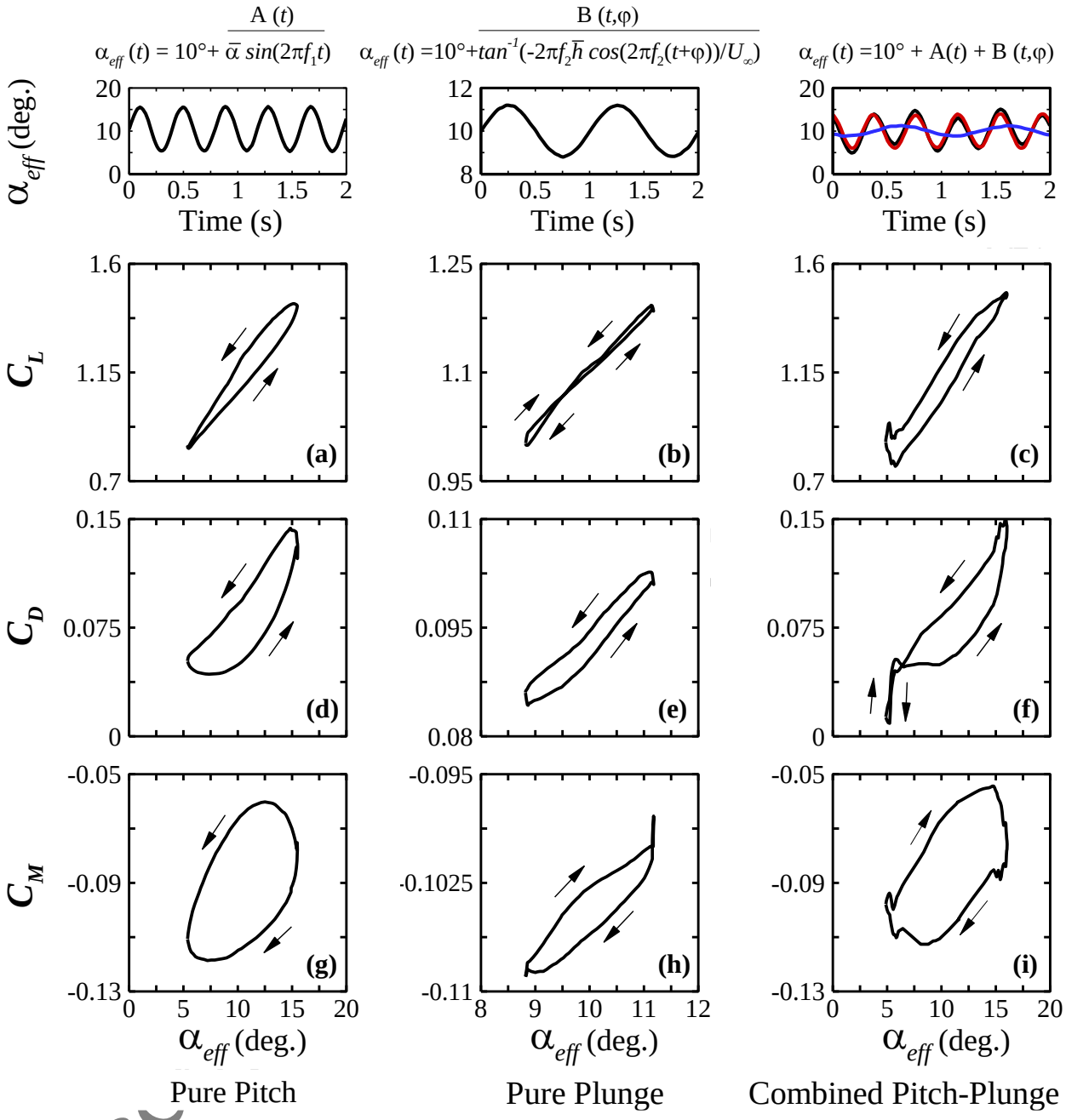

Figure 6 Measured hysteresis curves of aerodynamic coefficients for pure pitch, pure plunge and combined pitch-plunge motions

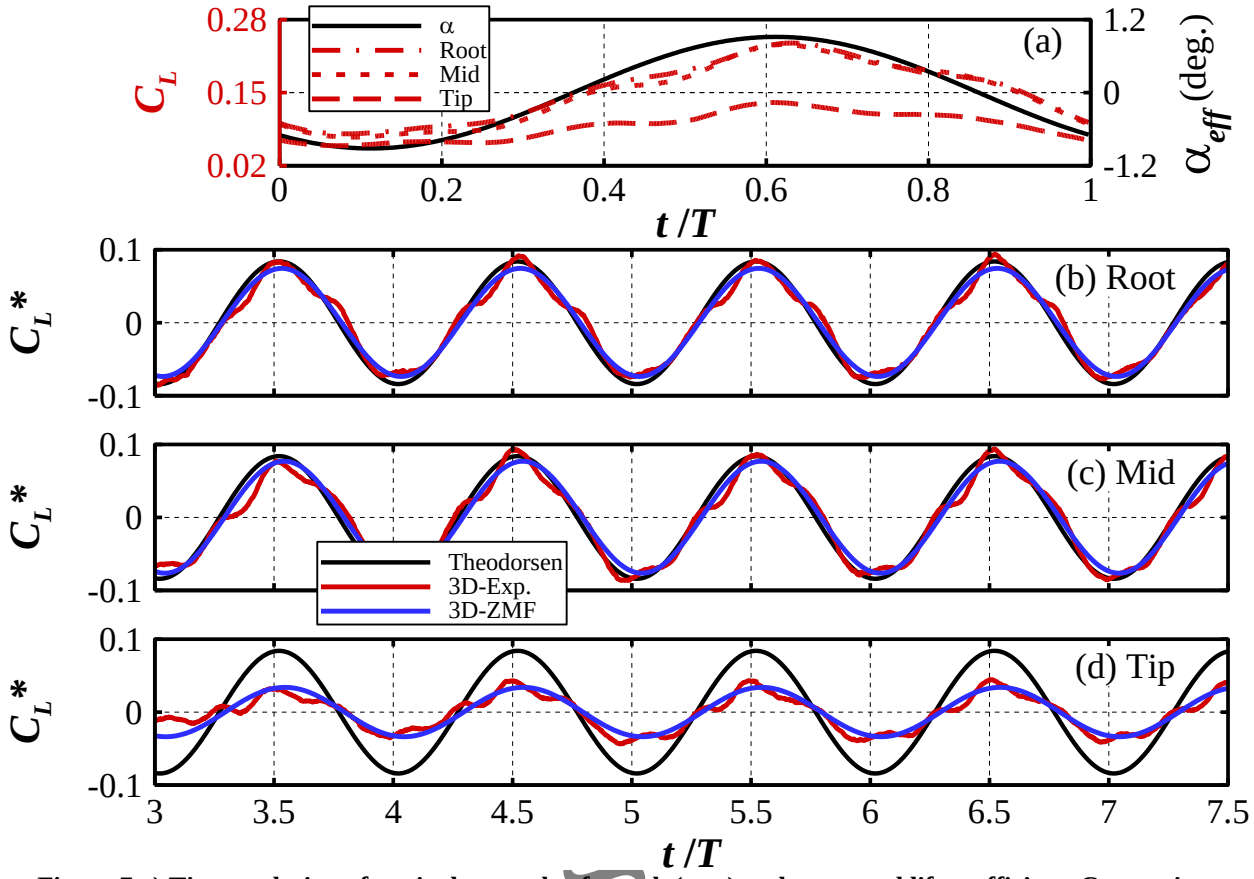

Figure 7 a) Time evolution of equivalent angle of attack (α_{eff}) and measured lift coefficient. Comparison of time evolution of zero-mean value of measured and analytical lift coefficient for b) root-section, b) mid-section and c) tip-section ($\bar{h}/c = 0.1$, $k = 0.07$ and $\alpha_0 = 0^\circ$)

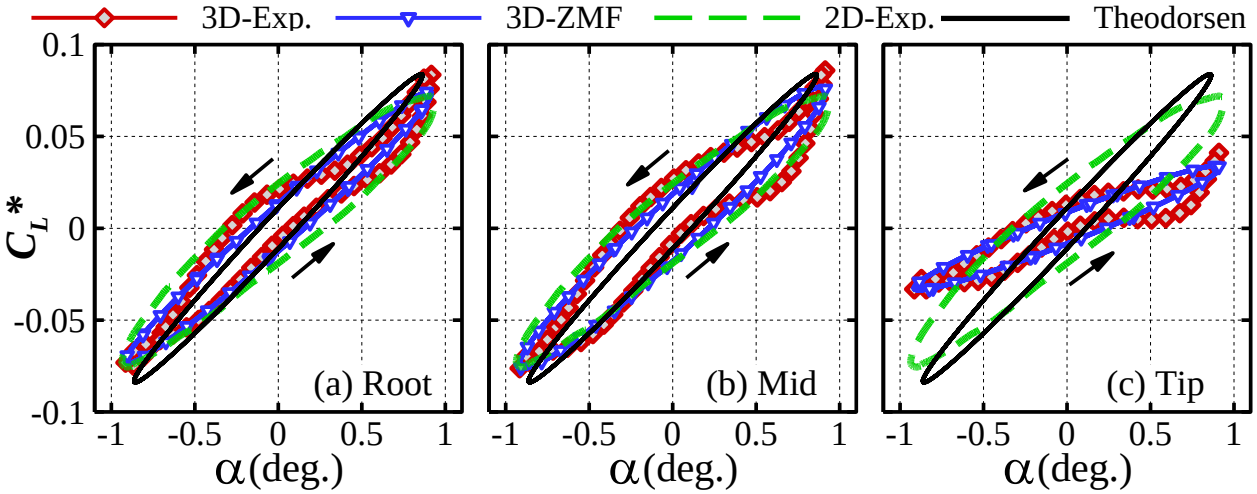

Figure 8 a) Measured lift coefficient hysteresis. Comparison of hysteresis of zero-mean value of measured and analytical lift coefficient for a) root-section, b) mid-section and c) tip-section ($\bar{h}/c = 0.1$, $k = 0.07$ and $\alpha_0 = 0^\circ$)

Mohammad BadrGoltape received his M.Sc. degree in aerospace engineering from Sharif university of technology in 2015, and he is a Ph.D. candidate at Sharif university of technology since 2015. He is currently a Ph.D. candidate in the Aerospace engineering of Sharif university of technology. His research interests include experimental aerodynamic, mechanical manufacturing, mechanism design and propulsion system design.

Mohammad Farahani is an Associate Professor in the Aerospace Engineering Department of Sharif University of Technology, Tehran, Iran. He has a PhD in Propulsion from Sharif University of Technology. His research interests include applied aerodynamics, unsteady aerodynamics, wind tunnel testing, gas dynamics, and turbo machinery.